



OPEN ACCESS

EDITED BY

Carmen Castro,
University of Cádiz, Spain

REVIEWED BY

Yuyao Tian,
The Chinese University of Hong Kong,
China
Grzegorz Wegrzyn,
University of Gdansk, Poland

*CORRESPONDENCE

Francesco M. Piccolo,
✉ fpiccolo@rockefeller.edu
Ali H. Brivanlou,
✉ brvnlou@rockefeller.edu

[†]These authors share last authorship

RECEIVED 03 July 2023

ACCEPTED 14 August 2023

PUBLISHED 01 September 2023

CITATION

Laundos TL, Li S, Cheang E, De Santis R,
Piccolo FM and Brivanlou AH (2023),
Huntingtin CAG-expansion mutation
results in a dominant negative effect.
Front. Cell Dev. Biol. 11:1252521.
doi: 10.3389/fcell.2023.1252521

COPYRIGHT

© 2023 Laundos, Li, Cheang, De Santis,
Piccolo and Brivanlou. This is an open-
access article distributed under the terms
of the [Creative Commons Attribution
License \(CC BY\)](https://creativecommons.org/licenses/by/4.0/). The use, distribution or
reproduction in other forums is
permitted, provided the original author(s)
and the copyright owner(s) are credited
and that the original publication in this
journal is cited, in accordance with
accepted academic practice. No use,
distribution or reproduction is permitted
which does not comply with these terms.

Huntingtin CAG-expansion mutation results in a dominant negative effect

Tiago L. Laundos^{1,2,3,4}, Shu Li¹, Eric Cheang¹, Riccardo De Santis¹,
Francesco M. Piccolo^{1*†} and Ali H. Brivanlou^{1*†}

¹Laboratory of Synthetic Embryology, The Rockefeller University, New York City, NY, United States,

²ICBAS—Instituto de Ciências Biomédicas Abel Salazar, Universidade do Porto, Porto, Portugal,

³IS—Instituto de Investigação e Inovação em Saúde, Universidade do Porto, Porto, Portugal,

⁴INEB—Instituto de Engenharia Biomédica, Universidade do Porto, Porto, Portugal

Introduction: Huntington's disease (HD) remains an incurable and fatal neurodegenerative disease long after CAG-expansion mutation in the huntingtin gene (*HTT*) was identified as the cause. The underlying pathological mechanism, whether *HTT* loss of function or gain of toxicity results from mutation, remains a matter of debate.

Methods: In this study, we genetically modulated wild-type or mutant *HTT* expression levels in isogenic human embryonic stem cells to systematically investigate their contribution to HD-specific phenotypes.

Results: Using highly reproducible and quantifiable *in vitro* micropattern-based assays, we observed comparable phenotypes with HD mutation and *HTT* depletion. However, halving endogenous wild-type *HTT* levels did not strongly recapitulate the HD phenotypes, arguing against a classical loss of function mechanism. Remarkably, expression of CAG-expanded *HTT* in non-HD cells induced HD like phenotypes akin to *HTT* depletion.

Discussion: By corollary, these results indicate a dominant negative effect of mutated *HTT* on its wild-type counterpart. Complementation with additional copies of wild-type *HTT* ameliorated the HD-associated phenotypes, strongly supporting a classical dominant negative mechanism. Understanding the molecular basis of this dominant negative effect will guide the development of efficient clinical strategies to counteract the deleterious impact of mutant *HTT* on the wild-type *HTT* function.

KEYWORDS

Huntington's disease (HD), *Huntingtin* (*HTT*), human embryonic stem cell (hESC), dominant negative, organoids

1 Introduction

Huntington's disease (HD) is a heritable, fully penetrant, autosomal neurodegenerative disease caused by a CAG trinucleotide expansion within the first exon of the *Huntingtin* (*HTT*) gene (Macdonald, 1993), leading to an expanded polyglutamine (polyQ) stretch at the N-terminal portion of the encoded *HTT* protein. Expansions above 35CAG are in the pathological range (Kay et al., 2016), and age of clinical onset correlates with CAG repeat length, with larger expansion leading to earlier onset of motor symptoms (Andrew et al., 1993; Duyao et al., 1993). Due to selective neuronal vulnerability, pathological CAG

expansion on the *HTT* gene (hereafter also referred to as HD mutation) results in extensive loss of striatal medium spiny neurons and cortical neurons, a disease hallmark evident in *postmortem* HD patient brains (Aylward et al., 2011; Halliday et al., 1998; Ross and Tabrizi, 2011). Three decades since the genetic cause was identified, the molecular mechanism by which a monoallelic mutation results in disease onset in adults is yet to be fully understood, and a cure or treatment to stop the progression of the disease is currently non-existent.

HTT protein is ubiquitously expressed in all tissues from the early embryo onwards, and despite its function being still largely elusive, it has been suggested to participate in a variety of cellular processes, such as vesicle transport (Caviston et al., 2007), ciliogenesis (Haremaki et al., 2015), cell survival (Zhang et al., 2006), and establishment of polarity (Galgoczi et al., 2021). Animal models showed that lack of *HTT* expression is embryonically lethal at day E7.5 (Duyao et al., 1995) and there have been no reports of healthy human patients devoid of *HTT* expression. Furthermore, mouse forebrain-specific knockout of *HTT* results in progressive neurodegeneration (Dragatsis et al., 2000), suggesting that *HTT* is required both for proper embryonic development and for maintenance of the neuronal population.

While several mouse models have been generated to recapitulate some of the hallmarks of HD pathophysiology, such as loss of striatal neurons and motor dysfunction [reviewed in (Figiel et al., 2012)], they pose limitations due to interspecies differences and a lack of a complete phenotype. Alternatively, *in vitro*, it has been shown that HD mutation results in neuronal dysfunction, such as altered axonal transport of BDNF, abnormal mitochondrial dynamics, and mitotic spindle orientation (Gauthier et al., 2004; Shirendeb et al., 2012; Lopes C. et al., 2016). However, the severity of these phenotypes associated with HD mutation are challenging to quantitatively attribute to the various CAG lengths and *HTT* expression levels, hindering clarification of the mechanism behind HD clinical presentation. Thus, the consequences of HD mutation on the physiological function of *HTT* remain mostly unknown.

Our laboratory has previously generated a series of micropattern-based *in vitro* assays, which unveiled novel and subtle HD-signature phenotypes in standardized and reproducible spatially-confined cultures with defined geometry that are well-suited for direct quantitative measurements of the spatial organization of cells.

Although these micropatterned human embryonic stem cell (hESC) assays pose inherent limitations, not fully replicating neurodegeneration observed in Huntington's Disease, they have demonstrated their usefulness in understanding basic *HTT* biology and of its mutant forms. Besides revealing new HD-associated phenotypes, these assays proved to be highly sensitive and specific by displaying increased phenotypic severity correlating with CAG domain expansion level (Haremaki et al., 2015; Ruzo et al., 2018; Galgoczi et al., 2021; Piccolo et al., 2022). Additionally, the quantification of these phenotypes has established that lack of *HTT* expression invariably recapitulates the signatures observed in CAG expanded lines with the highest degree of severity, suggesting that CAG expansion mutation might result in the progressive loss of *HTT* functions.

In this study, our aim is to systematically assess the effect of HD mutation on *HTT* function and directly test the hypothesis that the

observed phenotypes are due to loss of *HTT* function. We achieve this by employing two alternative micropattern-based assays: 1) a fast signaling readout assay, consisting of 1 h of activin A stimulation of confluent pluripotent cells so that, in WT control condition, only cells at the edge of the colony are activated due to the baso-lateral localization of the activin A receptor, rendering them inaccessible to its ligand activin A at the center; conversely, the HD-signature consists in the activation of most cells regardless of their geometrical positioning, due to impaired polarity and receptor mislocalization (Galgoczi et al., 2021); 2) a long-term assay, neuruloid formation in a 7-day culture, which models the self-organization of major ectodermal lineages during human neurulation and where the HD-signature phenotype results in failed compaction of the central neural ectodermal domain and in the reduction of the neural crest lineage (Haremaki et al., 2019). These are highly reproducible standardized culture systems that allow accurate quantitative assessment of small phenotype changes.

Using these two assays, we show that a halved level of *HTT* expression results in a very mild HD-like phenotype, significantly less severe than in HD hESCs. Moreover, we show that the expression of a mutant *HTT* (m*HTT*) transgene in WT cells containing a full dose of endogenous wt*HTT* results in the induction of a HD phenotype, mimicking the phenotypes observed in HD monoallelic mutation and in *HTT*^{-/-} cells. This indicates that m*HTT* has a deleterious effect on wt*HTT* activity. Moreover, genetic complementation of HD lines with exogenously expressed full-length wt*HTT* can rescue their phenotypes in micropattern-based assays, but not fully, suggesting HD mutation results in a dominant negative effect. Whether this effect occurs at the RNA or protein level, needs further investigation.

2 Results

2.1 Lowering *HTT* expression induces HD-signature phenotypes

To directly assess the consequences of CAG expansion mutation on *HTT* physiological function we compared the phenotypes of a HD hESC line, where one *HTT* allele carries a 72CAG expansion mutation (*HTT*^{72/20}, HD), with isogenic lines producing half of the physiological level of *HTT* protein due to monoallelic inactivation (*HTT*^{20/-}, heterozygous) or none due to biallelic inactivation of *HTT* gene (*HTT*^{-/-}, hereafter referred as *HTT*-KO) in hESC that we previously generated (Ruzo et al., 2018) (Figures 1A–C). In wild-type (*HTT*^{20/20}, WT) hESC confluent micropattern culture, following 1 h stimulation with activin A (Figure 1D), cells at the edge of the colonies were activated and accumulate SMAD2/3 in the nucleus in response to apical activin A induction (Figure 1E, F), while cells at the center of the micropattern colonies did not show nuclear translocation of SMAD2/3. On the other hand, and as previously shown (Galgoczi et al., 2021), micropattern colonies formed by HD lines lost the spatial restriction of sensitivity to activin A, allowing the response to the morphogen in cells residing at the center region of the micropatterns (Figure 1E, F). In this experimental setting, the heterozygous line (*HTT*^{20/-}) showed a very subtle increase in SMAD2/3 nuclear signal in the center of the colony and overall significant increase in the total number of SMAD2/3⁺ nuclei

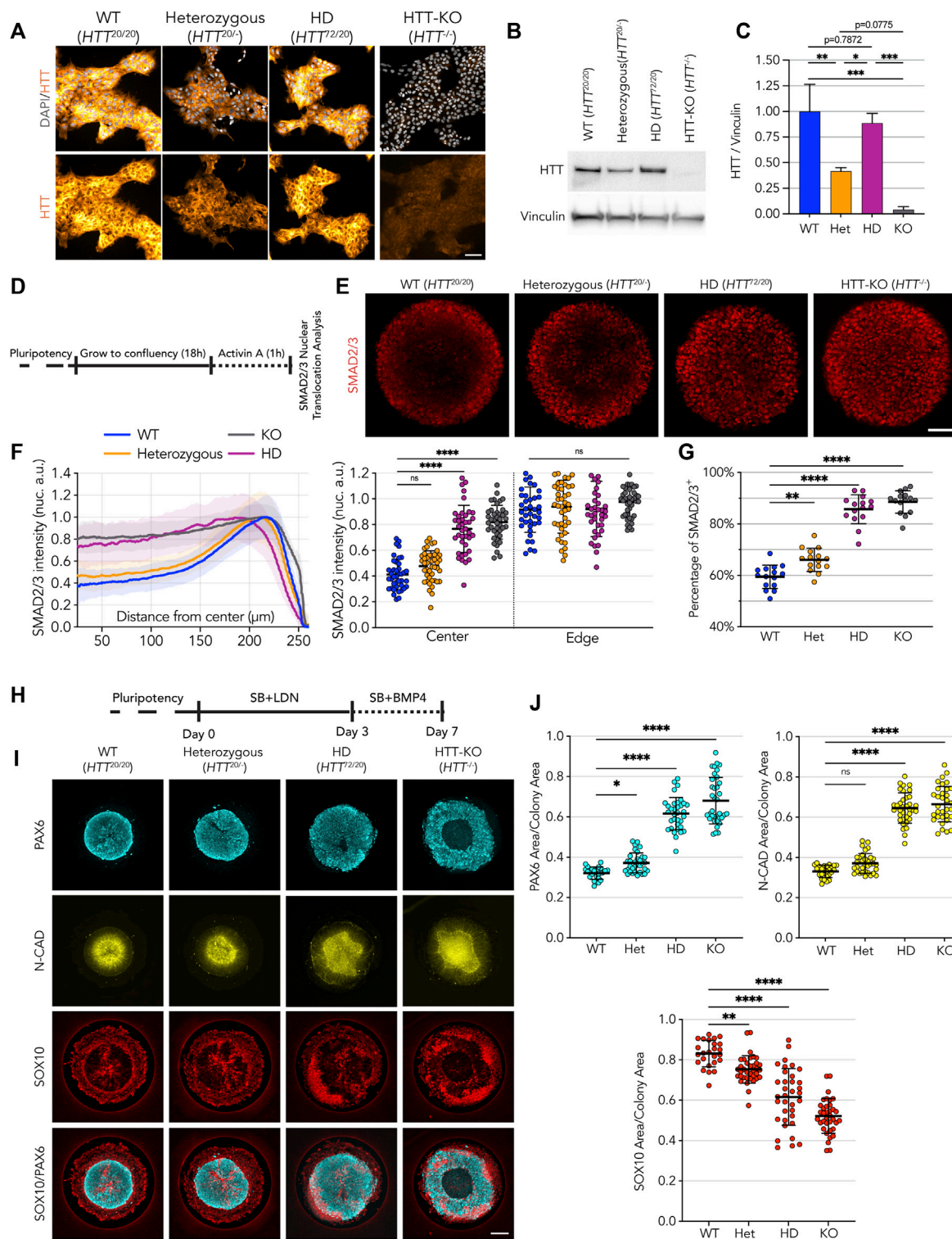


FIGURE 1

HD-signature phenotype in micropattern cultures show loss of *HTT* function. (A) Immunofluorescence detection of HTT protein in pluripotent embryonic stem cells illustrates reduction of HTT in heterozygous cell line (D7F7 antibody). HD cell line genetic makeup is *HTT*^{72/20}. (B) Immunoblot against HTT shows reduced HTT protein levels in heterozygous cell line (MAB2166 antibody). Vinculin shown as loading control. (C) Immunoblot signal quantification confirms halving of HTT protein amount compared to WT and HD lines (*n* = 3 independent experiments). (D) Schematics of activin A assay procedure performed on 500 μm circular micropatterns. (E) Immunofluorescence imaging shows SMAD2/3 nuclear translocation upon activin A stimulation, limited to the edges on WT and heterozygous colonies with wider to full induction on the colony center HD and HTT-KO colonies, respectively. (F) Mean radial intensity profile of nuclear SMAD2/3 shows insensitivity to activin A at the colony center in heterozygous cell lines is partially disrupted by lower *HTT* levels, with patches of activated cells in the colonies' center, in contrast with HD cell line which presents a phenotype comparable to HTT-KO with SMAD2/3 translocation induced throughout the micropatterned colonies (scatter plot displays the mean SMAD2/3 nuclear intensity for (Continued)

FIGURE 1 (Continued)

each colony at center:25-10 μm and edge:175 μm –225 μm ; WT $n = 41$, heterozygous $n = 44$, HD $n = 39$, KO $n = 41$) (G) Quantification of SMAD2/3⁺ nuclei numbers reveals an increase of the fraction of SMAD2/3⁺ in heterozygous cell lines, in line with a mild HD-like phenotype ($n = 15$ colonies per condition). (H) Schematics of the Neuruloid induction assay, performed on 500 μm circular micropatterns. (I, J) HTT protein halving in heterozygous cell line results in an enlarged neuroectodermal domain (PAX6 and N-CAD area) and a reduction of the neural crest lineage (SOX10 area). HD shows a significantly worsened phenotype than heterozygous cell line suggesting monoallelic CAG expansion on HD cell line does not result in from a classical loss of function of *HTT* upon mutation (WT $n = 25$, heterozygous $n = 33$, HD $n = 34$, KO $n = 36$). Groups were compared using one-way ANOVA followed by Dunnett's *post hoc* test for correction of multiple comparisons to the WT control (* $p < 0.05$, ** $p < 0.01$, *** $p < 0.001$, **** $p < 0.0001$, ns $p > 0.05$). All values are presented as mean \pm SD. a.u.: arbitrary units. Scale bar: 100 μm .

(Figure 1F, G), while lack of *HTT* expression (HTT-KO) resulted in the nuclear translocation of SMAD2/3 throughout the micropattern colony. This indicates that a reduced level of *HTT* expression results in an HD-signature phenotype, albeit significantly milder than complete lack of *HTT* expression or monoallelic HD mutation.

The consequences of lower *HTT* expression were also explored in the neuruloid formation assay (Figure 1H) (Haremakei et al., 2019). Here, HD hESC (*HTT*^{72/20}) showed a loosened central neuroectodermal domain, measured as an increased PAX6⁺ area and neural-cadherin (N-CAD) lumen, along with a contraction of the neural crest lineage, quantified as a decrease of the area occupied by SOX10⁺ cells (Figures 1I, J) (Haremakei et al., 2019). The neuruloids derived from the heterozygous (*HTT*^{20/-}) line, that express half of the physiological *HTT* level, displayed an HD-like phenotype in all three measurements. However, the extent of this phenotype was less severe than the phenotype observed in HD lines, which grossly failed to compact the central neuroectodermal area, a phenotype only worsened by complete lack of expression of *HTT*, as in the HTT-KO cell line (Figures 1F, G).

Taken together, these results show that reduced expression of *HTT* recapitulates aspects of the phenotypes observed in HD samples, suggesting that HD mutation might result in a loss of *HTT* function. However, when compared to the more severe HD phenotype, the milder HD-like phenotypes displayed by heterozygous cells provides evidence supporting the idea that monoallelic CAG expanded *HTT* might also exert deleterious activity that results in more severe phenotypes.

2.2 CAG-expansion affects *HTT* function

To dissect the effect of HD mutation on *HTT* function and its role in these platforms, we designed a transgenic system that allows us to modulate the expression of wild-type (wt*HTT*) and m*HTT* in the various isogenic backgrounds of the RUES2 HD allelic series (Ruzo et al., 2018). For this purpose, we engineered two PiggyBac vectors containing the coding sequence of full-length human *HTT* carrying a normal trinucleotide stretch (wt*HTT*, 20CAG), or an expanded CAG stretch (m*HTT*, 56CAG), expressed under the regulation of a constitutive promoter. At the 3' end of the *HTT* coding sequence, an in-frame sequence coding a Glycine-Serine flexible linker and the HaloTag coding sequence were introduced, resulting in a C-terminal tagging of the transgenic full-length *HTT* proteins (Figure 2A). These vectors (wt*HTT* or m*HTT*) were stably transfected into the HTT-KO cell line, and successful in-frame full-length expression was verified by immunoblot, with detection of the *HTT* protein as well as the HaloTag

amino acid sequences, confirming that the abundance of recombinant *HTT* protein resulting from the two transgenes in the generated cell lines were equivalent (Figure 2B; Supplementary Figure S3). To determine whether the HaloTag 3'-end/C-terminal fusion affects *HTT* activity, we tested for its ability to rescue the phenotype of HTT-KO hESCs in the two micropatterned-based assays. First, we performed the 1h activin A induction protocol where expression of wt*HTT* was able to rescue the phenotype of HTT-KO cells, resulting in a SMAD2/3 nuclear translocation restricted to edge of the micropatterns (Figure 2C, D). In contrast, expression of m*HTT* failed to rescue the HD-like phenotype of edge restricted SMAD2/3 activation (Figure 2C, D). Similarly, exogenous expression of wt*HTT* was also able to rescue the HD-like phenotype of HTT-KO hESC in the neuruloid assay, allowing for proper compaction of the central neuroectodermal region, measured as reduced area of the PAX6⁺ domain and the N-CAD⁺ lumina (Figures 2E, F), as well as rescue of the neural crest SOX10⁺ area. However, exogenous expression of full-length m*HTT* in HTT-KO hESC only led to partial rescue of its HD-like phenotype shown by a less pronounced reduction in the area PAX6⁺ and N-CAD⁺ domains, and milder increase in SOX10⁺ domain, indicating that in this more complex model, mutant *HTT* retains some activity for at least a partial rescue of the phenotype in cells devoid of *HTT* expression.

These results indicate that CAG-expansion might directly impair the function of *HTT*.

2.3 m*HTT* transgene insertion is sufficient to induce HD-like phenotype in wild-type hESCs

After assessing the functionality of wt*HTT* and m*HTT* transgenic insertion in HTT-KO hESCs, we exogenously expressed them in WT hESCs to directly test the effect of m*HTT* on the two micropattern assays (Figures 3A, B; note that recombinant *HTT*-Halotag proteins are ~33 kDa larger than endogenous wt*HTT* due to the C-Terminal tag). As a control, overexpression of transgenic wt*HTT* in WT hESCs did not affect the ability of WT cells to spatially restrict sensitivity to activin A upon 1 h of stimulation, with nuclear translocation of SMAD2/3 limited to the edges of their colonies (Figures 3C, D). Similarly, WT hESCs overexpressing wt*HTT* were able to generate neuruloids that properly form a compact central neuroectodermal structure (PAX6/N-CAD), which was surrounded by a well-formed neural crest structure (SOX10) (Figures 3E, F).

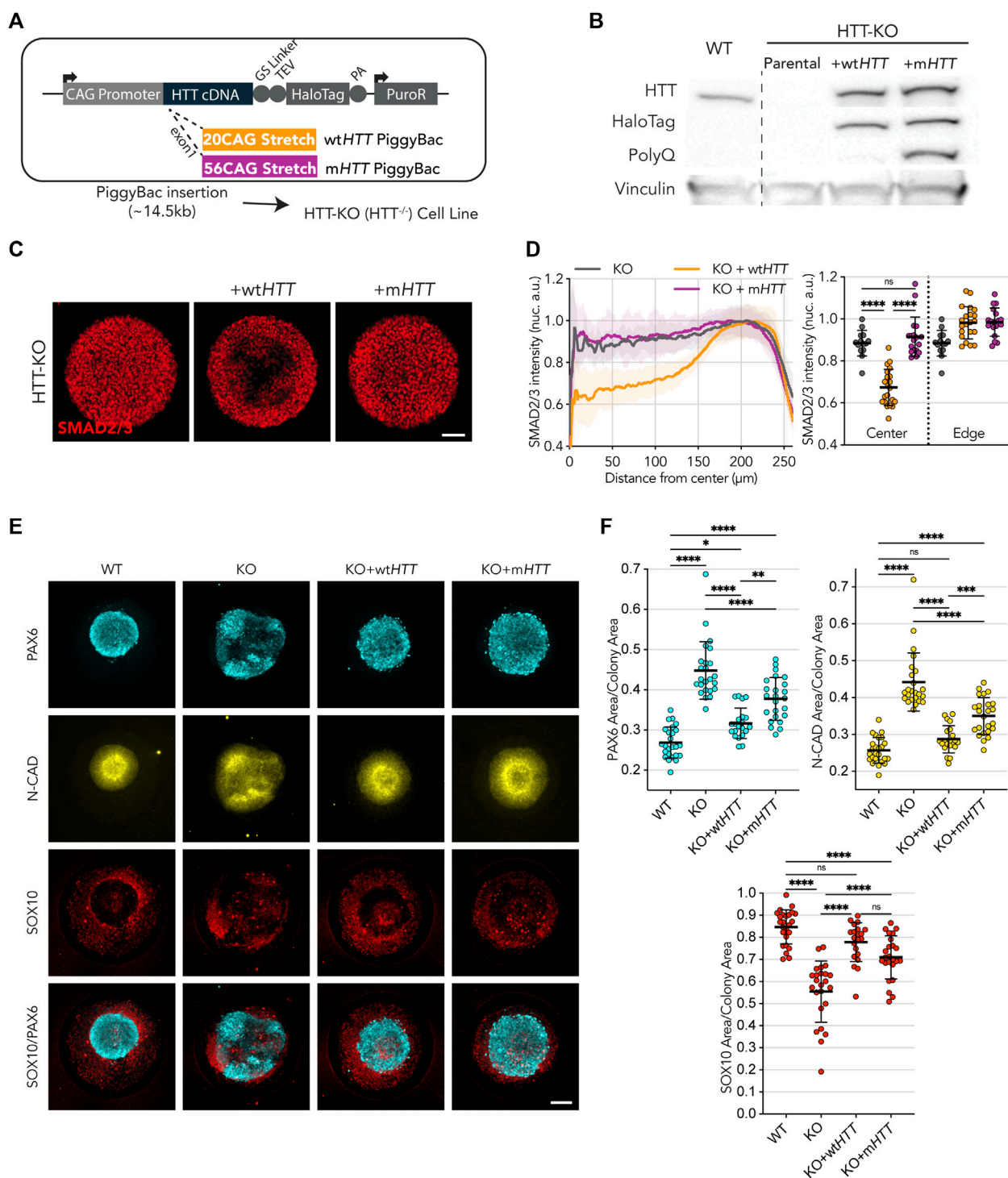


FIGURE 2

Wild-type *HTT*, but not mutant, restores endogenous *HTT* function. **(A)** Puromycin selectable PiggyBac transposon carrying the full-length *HTT* coding DNA sequence, to be expressed under the CAG promoter, and fused at the C-terminal with HaloTag spaced by a Glycine-Serine Linker for added flexibility. Two vectors were built to contain a 20CAG (wt) or 56CAG (mt) stretch on exon 1. The ~14.5 kb transposon was inserted into an *HTT*-KO cell line with ablated endogenous *HTT* expression. **(B)** Immunoblot against *HTT* (MAB2166) shows exogenous *HTT* protein expression in *KO*+*wtHTT* and *KO*+*mHTT*; *HTT* exogenous expression lines also present the HaloTag epitope around *HTT* size (~350 kDa) showing tag remains fused; mutant *HTT* transposon in *KO*+*mHTT* is detected with anti-PolyQ specific antibody (MW1). Vinculin shown as loading control. **(C)** Expression of exogenous *wtHTT* restores edge restriction in response to activin A in *HTT*-KO, with absence of SMAD2/3 nuclear translocation at the colony center (*KO*+*wtHTT*), an effect that is not observed with the mutant counterpart. **(C,D)** Mean radial intensity profile of nuclear SMAD2/3 confirms this effect (*HTT*-*KO* *n* = 14, *KO*+*wtHTT* *n* = 21, *KO*+*mHTT* *n* = 18). **(E,F)** Exogenous expression of *wtHTT*, and to a lesser extent of *mHTT*, results in a reduction of the neuroepithelial domain (PAX6 and N-CAD), as well as an increase in neural crest domain (SOX10) (WT *n* = 25, *HTT*-*KO* *n* = 24, *KO*+*wtHTT* *n* = 21, *KO*+*mHTT* *n* = 24). Groups were compared using one-way ANOVA followed by Tukey's *post hoc* test for correction of multiple comparisons (**p* < 0.05, ***p* < 0.01, ****p* < 0.001, *****p* < 0.0001, ns *p* > 0.05). All values are presented as mean ± SD. a.u.: arbitrary units. Scale bar: 100 μm.

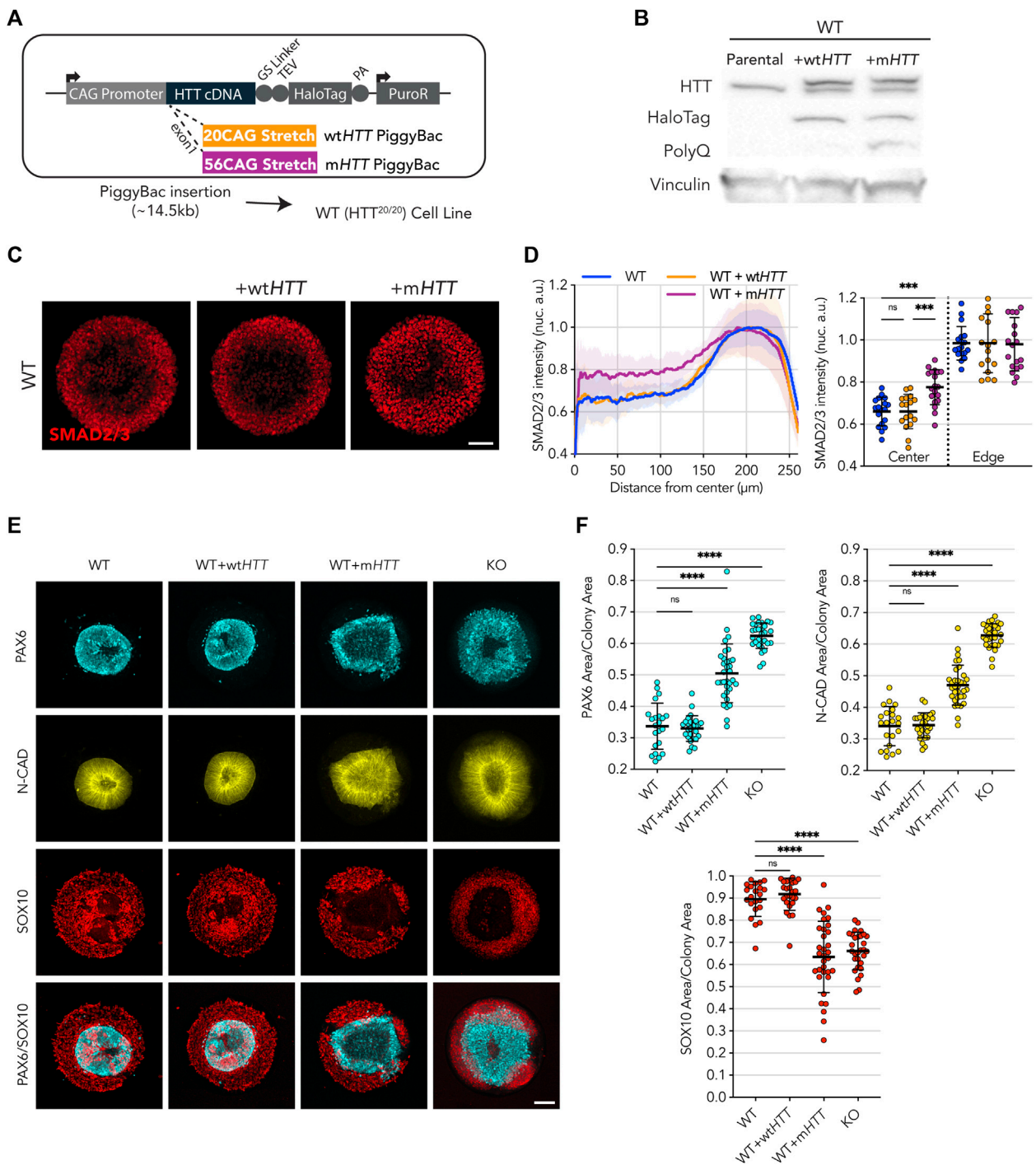
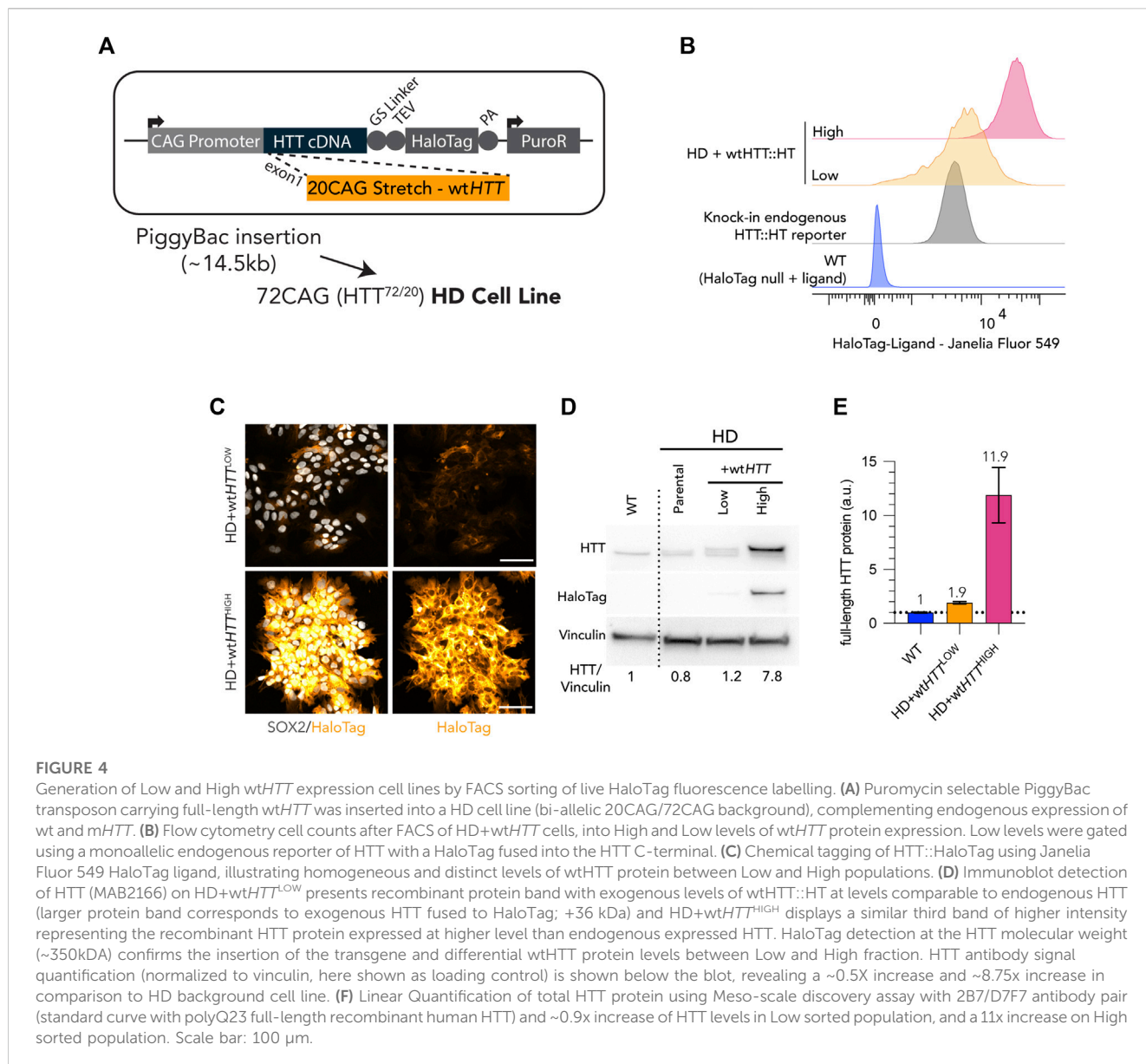


FIGURE 3

Transgenic expression of full-length *mHTT* induces HD phenotype in WT cell lines. **(A)** Puromycin selectable PiggyBac transposon carrying the full-length *HTT* coding DNA sequence and containing either 20CAG (*wtHTT*) or 56CAG (*mHTT*) stretch on exon 1 was inserted in a WT cell line, which originally expresses *wtHTT* protein at endogenous levels. **(B)** Immunoblot against *HTT* (MAB2166) shows endogenous levels of *HTT* across the 3 lines (~350 kDa); *WT+wtHTT* presents a second band corresponding to the recombinant *HTT::HaloTag* coded by the inserted transgene, at higher molecular weight than *wtHTT* due to the fusion to HaloTag (+33 kDa); *WT+mHTT* also presents a recombinant *mHTT::HaloTag* protein band, though at higher molecular weight than the former *wtHTT::HaloTag* recombinant protein due to the addition of the expanded polyglutamine stretch on the mutant version (additional 36 Glutamines; +12 kDa). HaloTag expression is confirmed for both exogenous *HTT* expression cell lines as well as specificity of PolyQ expansion on *WT+mHTT* cell line (MW1 antibody). Vinculin shown as loading control. **(C,D)** Mean radial intensity profile of nuclear SMAD2/3 reveals expression of exogenous *mHTT* in WT cells disrupts edge sensing restriction to activin A stimulation (1h), resulting in SMAD2/3 nuclear translocation in central areas of the micropattern in an HD like phenotype, while *wtHTT* overexpression did not impact the WT radial profile (*WT* *n* = 18, *WT+wtHTT* *n* = 17, *WT+mHTT* *n* = 19). **(E)** Neuruloid formation assay shows insertion of *mHTT* leads to increased PAX6/N-CAD neuroectodermal domain in a HD like Phenotype. **(F)** Quantification of confirms the increased PAX6 and N-CAD domain in WT cells presenting the *mHTT* transgene, as well as a reduction in the SOX10⁺ neural crest domain to a level seen in *HTT*-KO neuruloid suggesting a Dominant negative effect of *mHTT* on WT cells. Groups were compared using one-way ANOVA followed by Dunnett's *post hoc* test for correction of multiple comparisons to the WT control (**p* < 0.05, ***p* < 0.01, ****p* < 0.001, *****p* < 0.0001, ns *p* > 0.05). All values are presented as mean ± SD. a.u.: arbitrary units. Scale bar: 100 μm.



On the other hand, exogenous expression of *mHTT* profoundly affected the ability of WT hESCs to perform in the two micropattern assays. Upon 1 h of activin A stimulation, large patches of cells exhibiting nuclear translocation of SMAD2/3 appeared toward the center of the colony, reminiscent of the HD phenotype previously shown (Figures 3C, D). Likewise, in the neuruloid assay, a similar effect was observed with the micropatterns presenting grossly misshapen and enlarged central domains (as shown by PAX6 and N-CAD signal) as well as a reduction of the neural crest lineage (SOX10), recapitulating the phenotype previously characterized for the HD line (Figures 3E, F).

These observations show that the expression of a mutant form of *HTT* in a fully competent WT (*HTT*^{20/20}) background is sufficient to elicit HD-like phenotypes. This indicates that CAG expansion mutation on the *HTT* gene results in some kind of detrimental activity that might interfere with physiological processes performed by endogenous *HTT* in WT cells.

2.4 Genetic complementation with full-length *wtHTT* partially rescues the phenotypes of HD lines

Since exogenous expression of *mHTT* induces HD-like phenotypes in WT hESCs, while only partially rescuing the HD-like phenotypes of *HTT*-KO hESCs, we hypothesized that CAG expansion mutation might result in a reduced function of *HTT* and in some gained activity that somehow interferes with the physiological function of wild-type *HTT* gene products. To test this hypothesis, we sought to genetically complement an HD hESC line, carrying monoallelic 72CAG expansion mutation (*HTT*^{72/20}), with our construct encoding full length *wtHTT* and determine whether excess of *wtHTT* protein would rescue its HD-signature phenotypes (Supplementary Figure S4A). Stable protein translation of *HTT*-HaloTag was verified by *HTT* and HaloTag protein immunodetection (Supplementary Figures S4B, S4C).

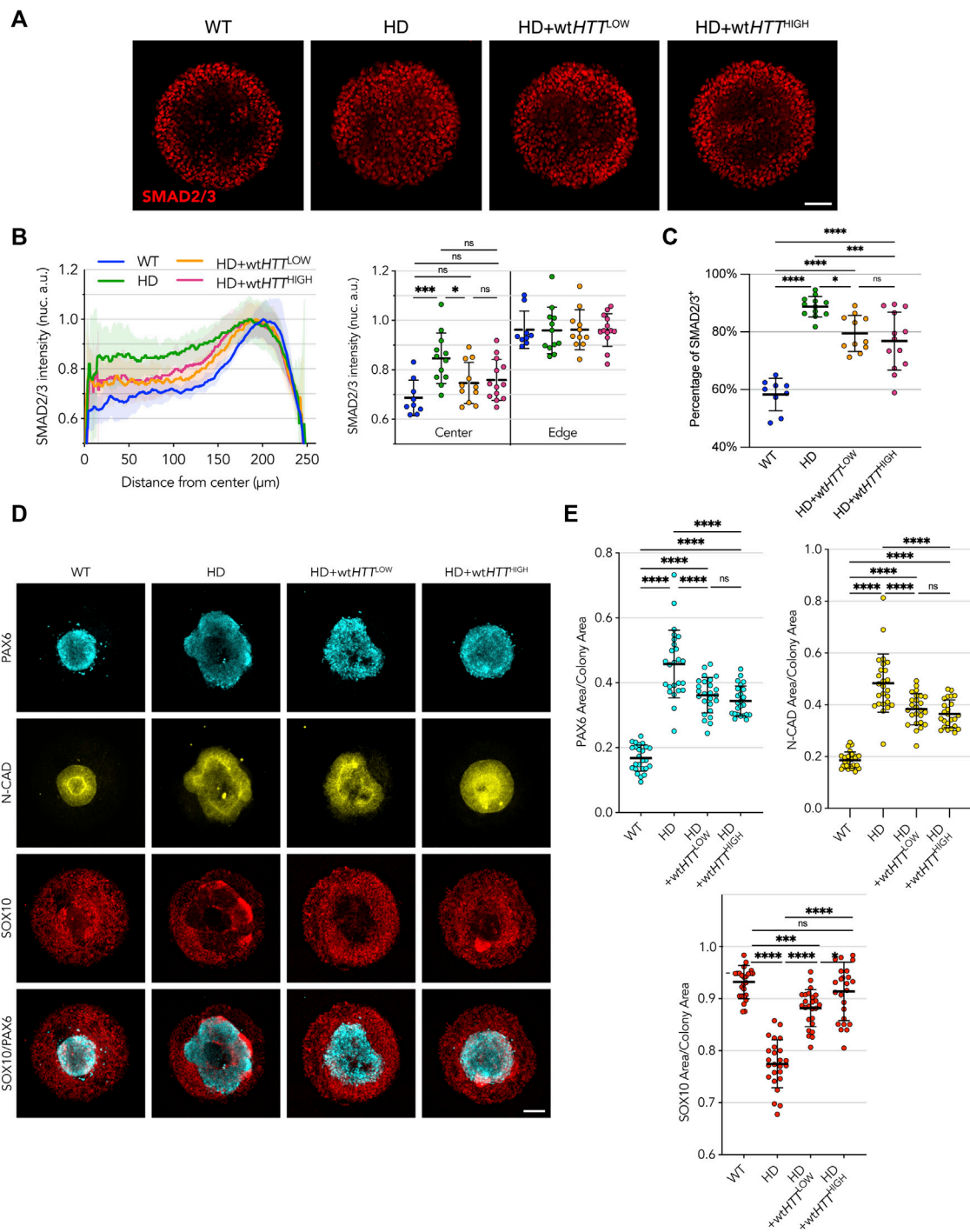


FIGURE 5

Homogeneous levels of wtHTT expression partially rescue the phenotype in HD cells, independent of expression level. (A) Upon activin A stimulation of 500 μm micropatterns, edge restriction of SMAD2/3 nuclear translocation is observed in HD cells complemented with both Low and High levels of wtHTT. (B) Radial profile analysis confirms this behavior, however, not to the levels observed in WT colonies. (C) Binary quantification of positive SMAD2/3 nuclei confirms a trend to amelioration of the phenotypes towards WT-like with increasing wtHTT dose. (D, E) wtHTT resulted in rescued compaction of PAX6/N-CAD neuroectodermal domain in the neuruloid assay and recovered SOX10 area. Groups were compared using one-way ANOVA followed by Dunnett’s *post hoc* test for correction of multiple comparisons (**p* < 0.05, ***p* < 0.01, ****p* < 0.001, *****p* < 0.0001, ns *p* > 0.05). All values are presented as mean ± SD. a.u.: arbitrary units. Scale bar: 100 μm.

Differently from the HTT-KO cell line, complementation of HD hESC lines with wtHTT partially, but significantly, rescued the HD phenotype on the activin A assay (Supplementary Figures S4D, S4E).

Likewise, on the neuruloid assay a similar partial rescue was observed, with the central neuroectoderm domain displaying an improved level of compaction, as shown by a smaller area of PAX6+

cells and N-CAD⁺ lumen, when compared to the parental HD cell line (Supplementary Figures S4F, S4G).

The partial improvement of the HD-signature phenotypes observed in these experiments provides evidence in support of the hypothesis of a dominant negative effect associated with HD mutation.

In the experimental context described above, the inability to fully rescue these phenotypes could be the result of a heterogeneous expression level of the exogenous wtHTT transgene or that a certain amount of extra wtHTT gene products might be required to overcome the dominant effect of endogenous mHTT. To address this possibility, we took advantage of the fused HaloTag in our recombinant HTT proteins (Figure 4A) to enrich for cells homogeneously producing low or high levels of wtHTT-HaloTag protein by fluorescence activated cell sorting (FACS) (Figure 4B). Thus, HD cells complemented with wtHTT-HaloTag were sorted for low levels of HTT (hereafter named as Low), equivalent to endogenous HTT protein level (determined by using a WT knock-in *HTT-HaloTag* reporter cell line as reference). A population of HD hESC complemented with wtHTT-HaloTag was also sorted for high level of the wtHTT recombinant protein and hereafter named as High (Figure 4B). HaloTag labelling confirmed that Low and High homogeneously express the transgene at two different levels (Figure 4C), also shown by immunoblot analysis (Figure 4D). Additionally, linear quantification by MesoScale Discovery Analysis showed that the amount of full-length wtHTT recombinant protein in Low is estimated as expected at ~2x the endogenous amount of HTT protein, and High at >10x the level measured in control WT (Figure 4E).

In the HD line complemented with both the Low and High wtHTT protein levels, SMAD2/3 nuclear translocation in response to activin A induction in micropattern cultures resulted in a pronounced WT-like phenotype ($p = ns$ vs. WT cells) (Figures 5A, B). Quantification of the percentage of SMAD2/3 nuclei showed that the number of cells responding to activin A stimulus decreased with overexpression of wtHTT, but without reaching the lower level of activated cells observed in WT colonies, regardless of the expression level of the transgene (Figure 5C). Additionally, the degree of rescue was equivalent for Low and High wtHTT levels, indicating that in the context of this assay, complementing an HD cell line with wtHTT only partially rescues the HD phenotype, independent of expression level.

In the neuruloid assay, complementation of the HD cell line with low levels of wtHTT was enough to elicit a rescue towards WT-like phenotype, with improved compact neuroectodermal (PAX6⁺) and N-CAD domains, as well as a larger neural crest SOX10⁺ domain than the parental HD line (Figures 5D, E). On the other hand, complementation with wtHTT protein at High levels resulted in a more pronounced rescue, both in extent of the compaction of the central neuroectoderm domain as well as its morphology, with colonies reaching full closure of the central area and rescue of the area occupied by neural crest cells.

Taken together, these results confirm the hypothesis that, at least partially, the HD signatures observed in a spatially confined pluripotent monolayer in response to activin A stimulation and in the neuruloid self-organization of ectoderm domains are the result of mHTT that acts in a dominant negative fashion. We show that CAG-expanded *HTT* expression impairs the normal function of wtHTT, and that mHTT impairment can be partially rescued with

increased expression of wtHTT, although never to a full extent even with levels as high as 10 times greater than the endogenous level.

3 Discussion

It has been three decades since HD was first described as a dominant monogenic disease linked to a polymorphic CAG trinucleotide tract in the *HTT* gene. While research has identified various abnormalities in normal cell and molecular functions as a result of HD mutation (Saudou and Humbert, 2016), because the clear function of *HTT* and its products is still poorly understood, the pathological mechanism resulting from the CAG expansion is still a matter of debate. Due to the presence of numerous confounding factors and the disease's human-specific nature, traditional approaches like human genetics and phenotypic characterization using animal models have been inadequate in fully resolving this issue. To study HD in humans, our lab generated a genetic allelic series of isogenic human ECS with increasing CAG lengths or *HTT* deletion (Ruzo et al., 2018) and applied them on an ensemble of micropattern-based assays that model different aspects of human development. Cellular and molecular changes due to HD mutation resulted in highly reproducible and quantifiable functional outputs, with phenotypic severity correlating with CAG length (Haremaki et al., 2019; Galgoczi et al., 2021), as observed with the age of HD onset in human patients.

Although the prevalent hypothesis suggests gain of toxic mechanisms as the cause of HD onset, a growing body of evidence suggests that loss of function might also be a contributing factor (Paine, 2015). *HTT* is ubiquitously expressed from fertilization onwards, with its expression becoming more pronounced in the nervous system (Saudou and Humbert, 2016). Lack of *HTT* expression results in arrested embryonic development at early stage (Duyao et al., 1995) and conditional deletion of *HTT* in adult mice forebrain and neurons cultured *in vitro* results in neuronal degeneration, motor phenotypes, early mortality, altered gene transcription and excitatory circuitry (Dragatsis et al., 2000; Zuccato et al., 2001; McKinstry et al., 2014; Braz et al., 2022; Wennagel et al., 2022). Additionally, we found that human HTT-KO ESC lines exhibited *in vitro* phenotypes comparable to CAG-expanded *HTT* cell lines with identical genetic backgrounds (Ruzo et al., 2018; Haremaki et al., 2019; Galgoczi et al., 2021), suggesting that the HD phenotypes might result of progressive loss-of-function with increasing CAG repeat tract length. Understanding the consequences of HD mutation on the physiological function of *HTT* is of primary importance for the design of effective clinical approaches for the treatment of the disease, and it lacked formal addressing.

In this study, we used a collection of human isogenic cell lines that vary in their HTT genetic makeup (WT 20CAG/20CAG, heterozygous 20CAG/-, HTT-KO -/-, and HD 72CAG/20CAG) to systematically investigate the genetic mechanism behind HD phenotypes in previously described *in vitro* micropattern-based assays of activin signaling transduction and self-organized neuronal organoids (Haremaki et al., 2015; Galgoczi et al., 2021). Here, haploinsufficiency (20CAG/-) did not fully recapitulate the HD-signature phenotypes previously described for HD (72CAG/20CAG) and HTT-KO hECSs in these assays (Figure 1), indicating

that the molecular insult due to the presence of mutant *HTT* in our model cannot be explained by a simple loss-of-function mechanism. Similar outcomes in both animal models and human patients were reported previously in other studies indicating that low amount of *HTT* expression is well tolerated and compatible with normal life. In fact, heterozygous mice with one null *HTT* allele and one hypomorphic *wtHTT* allele are embryonically viable and do not present any HD-associated phenotype (Murthy et al., 2019). Furthermore, lowering wild-type huntingtin by ~45% in the adult non-human primate striatum are phenotypically unremarkable for at least 6 months (Kaemmerer and Grondin, 2019). In the human population, *HTT* protein levels can vary at least 2-fold or more between different non-HD individuals (Fodale et al., 2022) and although cases of heterozygous individuals with only one functional copy of the *HTT* gene are rare, they can be found displaying no clinical HD presentation (Ambrose et al., 1994; Jung et al., 2021). Together, these findings are consistent with our results in supporting the idea that although lack of *HTT* expression results in HD-like outcome, intrinsic *mHTT* loss of activity would not be sufficient to elicit the HD-associated phenotypes.

In order to directly determine the effect of HD mutation on *HTT* function, we overexpressed full-length *mHTT* in *HTT*-KO hESCs showing that while it failed to rescue activin A signaling phenotype in micropatterned cultures, it was able to partially rescue the neuruloid phenotype confirming that indeed HD mutation inactivates (at least partially) the gene function (Figure 2). In agreement with this, it has been reported that HD mutation results in loss of *HTT* function in neurons (Gauthier et al., 2004). Moreover, other studies have shown that mouse embryonic lethality due to lack of *HTT* can be rescued with the expression of *mHTT* (White et al., 1997; Leavitt et al., 2001), suggesting that *HTT* protein retains at least partial function that is sufficient to overcome developmental arrest.

On the other hand, *mHTT* transgenic expression in fully competent WT hESCs efficiently induces HD phenotypes indicating that the HD phenotypes observed here are not due to simple inactivation of *mHTT* (Figure 3). The HD phenotypes we observe could then be explained as trans-inactivation of *wtHTT* protein by the co-expressed mutant *HTT* protein, resulting in a *HTT*-KO-like phenotype due to a dominant negative mechanism, which may have an effect proportional to the CAG repeat lengths (Ruzo et al., 2018; Harembaki et al., 2019; Galgoczi et al., 2021). Consistently, a report on a cis-regulatory variant in the *HTT* promoter that reduces its transcriptional activity showed that decreased *mHTT* expression delays the age of onset while reduction in *wtHTT* allele expression results in an earlier onset (Bečanović et al., 2015).

Considering this putative dominant negative mechanism, we attempted to rescue the HD phenotype in HD cells by increasing the levels of *wtHTT*. This resulted in a phenotypic amelioration in both micropattern assays, showing that we are indeed observing a deleterious effect of the *mHTT* on *wtHTT* function that can be overcome by increased *wtHTT* expression levels. However, by taking advantage of the two highly quantitative micropattern-based assays used, we observed that the phenotypic rescue of HD samples achieved by complementation with additional copies of *wtHTT* is only partial, even when *wtHTT* protein amounts were increased up to 10 times over endogenous levels (Figures 4, 5).

Opposing arguments to loss of function mediated by a dominant negative mechanism are that human patients with minimal or no *HTT* protein production due to either *HTT* aberrant splicing and/or post-translational mis-regulation of *HTT* RNA (e.g., LOMARS patients) present an extreme juvenile phenotype that differs from the progressive neurodegeneration observed in adult HD patients (Lopes F. et al., 2016; Jung et al., 2021). However, since severe pathology occurs in these patients at early age, it becomes very challenging to discern other brain alterations from complications ahead of normal HD progression. Additionally, even without considering the role of *mHTT* in HD, *wtHTT* protein loss is deleterious and therefore total *HTT* gene silencing therapies could result in worsened HD phenotype. In that regard, the Phase III GENERATION HD1 (NCT03761849) trial testing an antisense oligonucleotide targeting *HTT* mRNA was halted after preliminary analysis revealed that treatment resulted in unfavorable efficacy with worsening HD presentation compared to placebo groups (Schobel, 2021). While neuroinflammation or other adverse responses to the therapeutic agent could also explain this unfortunate outcome, one must consider the possibility of a dominant negative effect and therefore interpret the observed worsening of HD clinical manifestation as the consequences of lowered total *HTT* protein levels in HD patients, resulting in accelerated HD progression.

Overall, although we cannot exclude a component of pure gain of toxicity by *mHTT* protein product or its transcripts that might also contribute to HD pathogenesis, we show here by corollary that the hindering of *wtHTT* physiological function by *mHTT* (both in cis and trans) is at play in our system, and that the HD-associated phenotypes can be improved by complementation with additional copies of *wtHTT*, strongly supporting a classical dominant negative mechanism. A clear understanding of the molecular mechanisms behind the phenomenon we described here, or whether the observed toxic effect is attributable to the DNA, RNA, or protein level, is still lacking. However, because we could not fully rescue the phenotype with *wtHTT* overexpression and the dominant negative effect could not be explained by simple gain of toxicity of RNA transcripts, protein products or aggregates, we speculate that the dominant negative mechanism observed could be the result of *wtHTT*–*mHTT* protein crosstalk (either direct or indirect). In such scenario, formation of *mHTT* protein aggregates could also potentially sequester or hinder *wtHTT* protein dynamics and function in a dominant negative manner (Li et al., 2016). Future research will have to address how *wtHTT* biology is changed in the presence of its mutant counterpart, including but not limited to its protein interaction partners and its subcellular localization, which will provide the HD field with additional therapeutic targets to cure, ameliorate or halt progression of HD pathology. Until such advances are realized, increasing *wtHTT* levels could provide some degree of protection to HD patients. Alternatively, our results suggest that the most promising therapeutic approach at this stage should aim at allelic-specific silencing of the *mHTT* gene and targeted ablation of *mHTT* protein and its derivatives, despite the technical challenges to implement this universally.

4 Materials and methods

4.1 Human ES cell culture

Cell lines used in this study were derived from the RUES2 cell line, part of the NIH Human Embryonic Stem Cell Registry (RUES2-

NIHhESC-09-0013). hESCs were maintained in mouse embryonic fibroblast conditioned HUES Media in feeder-free conditions (conditioned media—CM), supplemented with bFGF 20 ng/mL, and replaced daily. hESCs were passaged at 70%–80% confluency every 3–4 days into Geltrex-coated dishes (Life Technologies) using Gentle Cell Dissociation Reagent (STEMCELL Technologies). Cells were tested for *Mycoplasma* spp. at 2-monthly intervals.

4.2 Stable integration of full-length HTT-HaloTag PiggyBac vectors in hESCs

Human ESCs were nucleofected using an Amaxa nucleofector II in Nucleofector Solution L (all Lonza) using B-016 preset. A total of 10^6 hESCs were nucleofected with 1 μ g of PiggyBac *HTT-HaloTag* plasmid (wtHTT or mHTT according to each experiment) and 1 μ g of the PiggyBac transposase (Lacoste et al., 2009). Cells were plated on Geltrex coated plates in CM supplemented with bFGF 20 ng/mL and 10 μ M ROCK-inhibitor (Y-27632) for 24 h. Cells were then selected with puromycin 1 μ g/mL for up to 10 days, and stable transfection validated by *in situ* labelling, flow cytometry, and immunoblot to confirm detection of HTT-HaloTag fused recombinant protein.

4.3 Immunoblotting

Protein was extracted on ice using ice cold RIPA Lysis and Extraction Buffer (Thermo Scientific 89900) supplemented with 1x Halt™ Protease and Phosphatase Inhibitor Cocktail (Thermo Scientific 78441). Cell lysates were briefly sonicated using a Branson Sonifier 450 (VWR; output 4, duty-cycle 10%, allowing 5 bursts) and incubated on ice for 15 min. Lysates were cleared by centrifuging at 12,000 rpm for 5 min at 4°C and protein concentration determined using the Pierce™ BCA Protein Assay (Thermo Scientific 23225). Samples were prepared for SDS-PAGE in 1x NuPAGE™ LDS Sample Buffer containing 50 mM DTT, boiled at 95°C for 5 min and loaded into a NuPAGE 3%–8% Tris-Acetate Gel (Thermo Scientific) along with HiMark™ Pre-stained Protein Standard (Thermo Scientific LC5699). Electrophoresis was run on ice and under stirring for 1h30 at 150 V. Protein bands were transferred to a Trans-Blot Turbo 0.2 μ m PVDF membrane (Bio-Rad Cat.#: 1704156) using a Trans-Blot Turbo Transfer System (Bio-Rad) and membranes blocked in Tris-buffered saline containing 0.1% Tween-20 (TBS-T) and 5% milk for 30 min. Primary antibodies were incubated overnight at 4°C (see Table S1 for antibody information) and HRP secondary antibodies for 30 min at RT. All incubations were carried under constant agitation and washed thoroughly between steps. HRP was detected using either Clarity or Clarity Max ECL Western blotting Substrates (Bio-Rad) and chemiluminescence detected in a Chemidoc MP system (Bio-Rad).

4.4 Activin A 2D micropattern assay

Spatially confined hESC response to activin A was performed as previously described (Galgoczi et al., 2021). Briefly, custom

micropatterned glass coverslips presenting 500 μ m growth areas (CYTOOCHIPS Arena 500A) were covered with 800 μ L of 10 μ g/mL recombinant human laminin 521 (BioLamina) diluted in PBS^{+/+}(Gibco) for 3 h at 37°C. Coated coverslips were transferred to 35 mm dishes containing 5 mL of PBS^{+/+} and serially washed 5 times, avoiding full removal to avoid drying, followed by one final complete wash with PBS^{+/+}. Cells lines were precultured in parallel to ensure similar growth upon the start of the assay. hESCs were dissociated in single cells using Accutase (STEM CELL Technologies) and 0.8×10^6 cells seeded per micropattern in 3 mL of CM with 20 ng/mL bFGF, 100 μ g/mL Normocin (InvivoGen), ROCK inhibitor and Y27632 (10 μ M; Abcam ab120129). Micropatterns were left unperturbed for 10 min to ensure homogenous distribution across the patterns and then transferred to 37°C. ROCK inhibitor was removed 3 h after seeding and upon 18 h incubation, the monolayers were induced with 100 ng/mL of activin A (R&D Systems). After 1 h incubation, samples were washed, fixed, and processed for immunofluorescence.

4.5 Neuruloid micropattern assay

Neuruloid culture (Haremaki et al., 2019) was performed in coated 500 μ m micropatterns as described above. Briefly, 0.5×10^6 cell were seeded per micropattern and incubated for 3 h at 37°C in HUES medium supplemented with 20 ng/mL bFGF, 10 μ M ROCK inhibitor Y27632 and 100 μ g/mL Normocin. Cultures were kept in Normocin for the whole experiment. The seeded micropatterns were then washed once with PBS^{+/+} and day 0 initiated in HUES with 10 μ M SB431542 and 0.2 μ M LDN 193189. On day 3, media was replaced with HUESM containing 10 μ M SB431542 and 3 ng/mL BMP4, with media replenished at day 5. Micropattern cultures were then fixed at day 7 and processed for immunofluorescence analysis.

4.6 Immunofluorescence

Cells were fixed with 4% paraformaldehyde (Electron Microscopy Sciences 15713) for 30 min at RT, washed thrice with PBS and permeabilized and blocked DPBS containing 0.5% Triton-X 100 (Sigma 93443) and 3% Normal Donkey Serum for 30 min. Primary antibody staining was performed in DPBS with 0.1%TX-100 (PBST) for 1 h 30 at room temperature, washed thrice with PBST for 5 min each, and secondary antibody staining was performed for 1 h in PBST at RT. After 2 washes with PBST and 1 PBS wash, samples were counterstained with 0.1 μ g/mL DAPI (Thermo Fisher Scientific D1306) for 10 min and washed. Micropattern coverslips were mounted on slides using ProLong Gold antifade mounting medium (Molecular Probes P36934). hESCs grown in IBIDI slides were mounted in IBIDI mounting medium and stored at 4°C before imaging. Antibodies used can be found in Table S1.

4.7 Fluorescence activated cell sorting (FACS)

Cells grown under confluency were incubated in CM+bFGF media containing 1 μ M cell permeable Janelia Fluor® 549 HaloTag ligand complex (Promega, GA1110) for 1 h at 37°C. Cells were

washed 3 times with PBS^{+/+} and incubated with fresh media to allow unbound ligand to be fully removed for 3 h. Monolayers were washed again with PBS^{-/-}, dissociated with Accutase and resuspended in PBS^{-/-}, containing HEPES 10 mM, EDTA 5 mM, BSA 0.5%. Duplets were excluded based on FSC-W and SSC-W gating and DAPI was used at 20 ng/mL for cell death exclusion. Cells were sorted in a FACS Aria Flow Cytometer (BD) using a 100 μ m/20psi nozzle. An endogenous C-terminal tagged CRISPR HTT reporter with HaloTag (unpublished) was used to define the gating for Low levels of HTT protein, and High levels were defined as all cells above that threshold. The parental untagged cell line was treated with HaloTag ligand in parallel and used as negative control. Cells were allowed to recover after sorting in Normocin and the obtained populations analyzed by flow cytometry, Western blot and HTT MSD quantification.

4.8 Electrochemiluminescence meso scale discovery for HTT protein quantification

To quantify total HTT protein levels on the generated cell lines, about 3×10^6 cells were pelleted and flash frozen in triplicates and sent for contracted analysis at Evotech with MSD assay CHDI_HTT_144 (antibody pair 2B7/D7F7) following SOP. Briefly, samples were lysed in ice cold MSD Tris Lysis Buffer and incubated 30 min at 4°C by rotating. After lysis, the samples were centrifuged (15700 rcf, 4°C; 6 min) and protein concentration determined with BCA assay and adjusted to 0.2 mg/mL, further diluted to 0.1 mg/mL in blocking buffer. Final buffer conditions for HTT quantitation assays were 20 mM Tris (pH 7.5), 150 mM NaCl, 1 mM EDTA, 1 mM EGTA, 1% Triton-X, 1x phosphatase inhibitor I and II (Sigma), complete mini EDTA free protease inhibitor cocktail tablet (Roche), 0.5 mM PMSF, 10 mM NaF. Purified recombinant full-length 1-3144 protein of human Huntingtin protein with 23 polyglutamine (CHDI-90001858) was used as standard, ranging between 0.001 and 10 fmol/ μ L.

4.9 HaloTag *in vitro* ligand staining

For imaging, hESCs were grown on glass surfaces previously coated with 10 μ g/mL recombinant human laminin 521 (BioLamina) diluted in PBS^{+/+} (Gibco) for 3 h at 37°C. Freshly thawed Janelia Fluor[®] 549 HaloTag[®] Ligand (Promega, GA1110) was diluted to 200 nM in warmed CM and cells incubated for 30 min. After washing thrice with PBS^{+/+}, cells were incubated for 30 min to allow unbound ligand to wash. Cells were then fixed in 4% PFA, nuclei counterstained with DAPI and imaged by confocal microscopy.

4.10 Imaging

Confocal microscope images of hESCs and neuruloid IF, were acquired with a 10x or 20 \times /0.8 NA dry objective lens (Zeiss), using 405, 488, 561, and 633 nm laser lines, and a combination of PMT and GaAsP detectors (LSM 780, Zeiss). Large tiled imaged were

obtained to sample the neuruloid assay. Activin A assay was imaged acquiring large tiled areas with an inverted wide-field epifluorescence microscope using 10 \times /0.45 NA dry objective lens (Zeiss Axio Observer Z1).

4.11 Image analysis

Fiji (2.0.0/1.53t) was used to stitch tiled images and to generate maximum projections of the generated confocal z-stacks. SMAD2/3 radial intensity profiling was performed as previously described with slight changes (Galgoczi et al., 2021). Briefly, using a custom Python script, a foreground mask was created to detect colonies by thresholding the DAPI channel and calculating alpha shapes with respect to predicted colony size, and colonies extracted into individual files. Ilastik (1.4.0b27, Berg et al., 2019) was then used to segment individual nuclei based on the DAPI channel. Identified nuclei were then filtered according to expected size to exclude debris and mitotic cells, and the center of the nuclear mask was determined for further watershed segmentation (scikit-image). The generated nuclear mask was then applied to the SMAD2/3 channel and median nuclear intensities were extracted, and SMAD2/3 radial profile was plotted according to each nucleus distance to the center of the colony. Profiles were normalized to 1 using the maximum value obtained in the profile.

To assess the total SMAD2/3 number, individual nuclei were segmented using Stardist (Schmidt et al., 2018; <https://arxiv.org/abs/1806.03535>), and the corresponding nuclear masks were used to calculate the mean intensity for each individual nucleus (scikit-image). Images were manually thresholded for SMAD2/3 to classify nuclear translocation as binary. The percentage of SMAD2/3 positive nuclei was then calculated on the total nuclei number.

Individual neuruloid images were obtained as explained above. Ilastik was used to segment the areas occupied by each marker and DAPI was used to determine the total neuruloid area. The pixel area for each marker was then determined and normalized as a fraction of the total DAPI area. Python libraries numpy, pandas, matplotlib and seaborn were used to organize the data and for plotting.

4.12 Statistics

All data presented in this study were obtained from at least two independent experiments. Statistically significant differences between conditions were determined using one-way analysis of variance (ANOVA) followed by Dunnett's *post hoc* test for correction of multiple comparisons. Statistical analyses were performed in Prism 9 (GraphPad). Results were considered not significant (ns) when the observed differences when $p > 0.05$, and significance levels were denoted as follows: * $p < 0.05$, ** $p < 0.01$, *** $p < 0.001$ and **** $p < 0.0001$.

Data availability statement

The raw data supporting the conclusion of this article will be made available by the authors, without undue reservation.

Author contributions

TL: study design, data acquisition and analysis, writing original draft. SL and EC: data acquisition. RDS: data analysis, review, and editing. FP: conceptualization, study design, supervision, writing original draft, review, and editing. AB: conceptualization, funding, supervision, review, and editing. All authors contributed to the article and approved the submitted version.

Funding

TL was supported by FCT PD/BD/127997/2016. TL (partially), FP, SL, EC, and AB were supported by the CHDI foundation (A-9423). RDS was supported by EMBO-LTF-254-2019.

Acknowledgments

We extend our sincere appreciation to the members of the Brivanlou lab for their valuable contributions and insightful discussions during this research. We are grateful for the support provided by the Rockefeller University Bio-Imaging Resource Center, particularly Alison North and Christina Pyrgaki, who offered exceptional assistance in microscopy. Special thanks are also due to the Flow Cytometry Resource Center and its team, including Svetlana Mazel, Stanka Semova, Samer Shalaby, and Songyan Han, for their technical expertise and guidance with the flow cytometry experiments. We acknowledge the early work on the full-length cDNA *HTT* PiggyBac plasmid by former lab members Albert Ruzo and Jeffrey Naftaly. We are also grateful to Jakob Metzger for

sharing and adjusting single cell quantification image analysis tools used for activin A radial quantification experiments. We want to express our sincere gratitude to Eleni Rice, Albert Jiang, and Andrew Beaudoin for their diligent and thorough proofreading of the manuscript. Additionally, we would like to express our appreciation to Tom Vogt, Dan Felsenfeld and David Howland from the CHDI Foundation for their valuable support and advice throughout this project.

Conflict of interest

AB is a co-founder and shareholder of RUMI Scientific.

The remaining authors declare that the research was conducted in the absence of any commercial or financial relationships that could be construed as a potential conflict of interest.

Publisher's note

All claims expressed in this article are solely those of the authors and do not necessarily represent those of their affiliated organizations, or those of the publisher, the editors and the reviewers. Any product that may be evaluated in this article, or claim that may be made by its manufacturer, is not guaranteed or endorsed by the publisher.

Supplementary material

The Supplementary Material for this article can be found online at: <https://www.frontiersin.org/articles/10.3389/fcell.2023.1252521/full#supplementary-material>

References

- Ambrose, C. M., Duyao, M. P., Barnes, G., Bates, G. P., Lin, C. S., Srinidhi, J., et al. (1994). Structure and expression of the Huntington's disease gene: evidence against simple inactivation due to an expanded CAG repeat. *Somat. Cell Mol. Genet.* 20 (1), 27–38. doi:10.1007/BF02257483
- Andrew, S. E., Paul Goldberg, Y., Kremer, B., Telenius, H., Theilmann, J., Adam, S., et al. (1993). The relationship between trinucleotide (CAG) repeat length and clinical features of Huntington's disease. *Nat. Genet.* 4 (4), 398–403. doi:10.1038/ng0893-398
- Aylward, E. H., Nopoulos, P. C., Ross, C. A., Langbehn, D. R., Pierson, R. K., Mills, J. A., et al. (2011). Longitudinal change in regional brain volumes in prodromal Huntington disease. *J. Neurology, Neurosurg. Psychiatry* 82 (4), 405–410. doi:10.1136/jnnp.2010.208264
- Bečanović, K., Nørremølle, A., Neal, S. J., Kay, C., Collins, J. A., Arenillas, D., et al. (2015). A SNP in the HTT promoter alters NF- κ B binding and is a bidirectional genetic modifier of Huntington disease. *Nat. Neurosci.* 18 (6), 807–816. doi:10.1038/nn.4014
- Berg, S., Kutra, D., Kroeger, T., Straehle, C. N., Kausler, B. X., Haubold, C., et al. (2019). Ilastik: interactive machine learning for (bio)image analysis. *Nature Methods* 16 (12), 12. doi:10.1038/s41592-019-0582-9
- Braz, B. Y., Wennagel, D., Ratié, L., de Souza, D. A. R., Deloulme, J. C., Barbier, E. L., et al. (2022). Treating early postnatal circuit defect delays Huntington's disease onset and pathology in mice. *Science* 377 (6613), eabq5011. doi:10.1126/science.abq5011
- Caviston, J. P., Ross, J. L., Antony, S. M., Tokito, M., and Holzbaur, E. L. F. (2007). Huntingtin facilitates dynein/dynactin-mediated vesicle transport. *Proc. Natl. Acad. Sci.* 104 (24), 10045–10050. doi:10.1073/pnas.0610628104
- Dragatsis, I., Levine, M. S., and Zeitlin, S. (2000). Inactivation of *Hdh* in the brain and testis results in progressive neurodegeneration and sterility in mice. *Nat. Genet.* 26 (3), 300–306. doi:10.1038/81593
- Duyao, M., Ambrose, C., Myers, R., Novelletto, A., Persichetti, F., Frontali, M., et al. (1993). Trinucleotide repeat length instability and age of onset in Huntington's disease. *Nat. Genet.* 4 (4), 387–392. doi:10.1038/ng0893-387
- Duyao, M. P., Auerbach, A. B., Ryan, A., Persichetti, F., Barnes, G. T., McNeil, S. M., et al. (1995). Inactivation of the mouse Huntington's disease gene homolog *hdh*. *Science* 269 (5222), 407–410. doi:10.1126/science.7618107
- Figiel, M., Szlachcic, W. J., Switonski, P. M., Gabka, A., and Krzyzosiak, W. J. (2012). Mouse models of polyglutamine diseases: review and data table. Part I. *Mol. Neurobiol.* 46 (2), 393–429. doi:10.1007/s12035-012-8315-4
- Fodale, V., Pintauro, R., Daldin, M., Spiezia, M. C., Macdonald, D., and Bresciani, A. (2022). Quantifying huntingtin protein in human cerebrospinal fluid using a novel polyglutamine length-independent assay. *J. Huntingt. Dis.* 11 (3), 291–305. doi:10.3233/JHD-220527
- Galgoczi, S., Ruzo, A., Markopoulos, C., Yoney, A., Phan-Everson, T., Li, S., et al. (2021). Huntingtin CAG expansion impairs germ layer patterning in synthetic human 2D gastruloids through polarity defects. *Development* 148 (19), dev199513. doi:10.1242/dev.199513
- Gauthier, L. R., Charrin, B. C., Borrell-Pagès, M., Dompierre, J. P., Rangone, H., Cordelières, F. P., et al. (2004). Huntingtin controls neurotrophic support and survival of neurons by enhancing BDNF vesicular transport along microtubules. *Cell* 118 (1), 127–138. doi:10.1016/j.cell.2004.06.018
- Halliday, G. M., McRitchie, D. A., Macdonald, V., Double, K. L., Trent, R. J., and McCusker, E. (1998). Regional specificity of brain atrophy in Huntington's disease. *Exp. Neurol.* 154 (2), 663–672. doi:10.1006/exnr.1998.6919
- Haremake, T., Deglincerti, A., and Brivanlou, A. H. (2015). Huntingtin is required for ciliogenesis and neurogenesis during early *Xenopus* development. *Dev. Biol.* 408 (2), 305–315. doi:10.1016/j.ydbio.2015.07.013
- Haremake, T., Metzger, J. J., Rito, T., Ozair, M. Z., Etoc, F., and Brivanlou, A. H. (2019). Self-organizing neuroblasts model developmental aspects of Huntington's disease in the ectodermal compartment. *Nat. Biotechnol.* 37 (10), 1198–1208. doi:10.1038/s41587-019-0237-5
- Jung, R., Lee, Y., Barker, D., Correia, K., Shin, B., Loupe, J., et al. (2021). Mutations causing Lopes-Maciel-Rodan syndrome are huntingtin hypomorphs. *Hum. Mol. Genet.* 30 (3–4), 135–148. doi:10.1093/hmg/ddaa283

- Kaemmerer, W. F., and Grondin, R. C. (2019). The effects of huntingtin-lowering: what do we know so far? *Degener. Neurological Neuromuscul. Dis.* 9, 3–17. doi:10.2147/DNND.S163808
- Kay, C., Collins, J. A., Miedzybrodzka, Z., Madore, S. J., Gordon, E. S., Gerry, N., et al. (2016). Huntington disease reduced penetrance alleles occur at high frequency in the general population. *Neurology* 87 (3), 282–288. doi:10.1212/WNL.0000000000002858
- Lacoste, A., Berenshteyn, F., and Brivanlou, A. H. (2009). An efficient and reversible transposable system for gene delivery and lineage-specific differentiation in human embryonic stem cells. *Cell Stem Cell* 5 (3), 332–342. doi:10.1016/j.stem.2009.07.011
- Leavitt, B. R., Guttman, J. A., Hodgson, J. G., Kimel, G. H., Singaraja, R., Vogl, A. W., et al. (2001). Wild-type huntingtin reduces the cellular toxicity of mutant huntingtin *in vivo*. *Am. J. Hum. Genet.* 68 (2), 313–324. doi:10.1086/318207
- Li, L., Liu, H., Dong, P., Li, D., Legant, W. R., Grimm, J. B., et al. (2016). Real-time imaging of Huntingtin aggregates diverting target search and gene transcription. *ELife* 5, e17056. doi:10.7554/eLife.17056
- Lopes, F., Barbosa, M., Ameer, A., Soares, G., Sá, J., Dias, A. I., et al. (2016). Identification of novel genetic causes of Rett syndrome-like phenotypes. *J. Med. Genet.* 53 (3), 190–199. doi:10.1136/jmedgenet-2015-103568
- Lopes, C., Aubert, S., Bourgeois-Rocha, F., Barnat, M., Rego, A. C., Déglon, N., et al. (2016). Dominant-negative effects of adult-onset huntingtin mutations alter the division of human embryonic stem cells-derived neural cells. *PLOS ONE* 11 (2), e0148680. doi:10.1371/journal.pone.0148680
- Macdonald, M. (1993). A novel gene containing a trinucleotide repeat that is expanded and unstable on Huntington's disease chromosomes. The Huntington's Disease Collaborative Research Group. *Cell* 72 (6), 971–983. doi:10.1016/0092-8674(93)90585-E
- McKinstry, S. U., Karadeniz, Y. B., Worthington, A. K., Hayrapetyan, V. Y., Ilcim Ozlu, M., Serafin-Molina, K., et al. (2014). Huntingtin is required for normal excitatory synapse development in cortical and striatal circuits. *J. Neurosci.* 34 (28), 9455–9472. doi:10.1523/JNEUROSCI.4699-13.2014
- Murthy, V., Tebaldi, T., Yoshida, T., Erdin, S., Calzonetti, T., Vijayvargia, R., et al. (2019). Hypomorphic mutation of the mouse Huntington's disease gene orthologue. *PLoS Genet.* 15 (3), e1007765. doi:10.1371/journal.pgen.1007765
- Paine, H. (2015). Does loss of the normal protein function contribute to the pathogenesis of Huntington's disease? *Biosci. Horizons Int. J. Student Res.* 8, hzv005. doi:10.1093/biohorizons/hzv005
- Piccolo, F. M., Kastan, N. R., Harembaki, T., Tian, Q., Laundos, T. L., De Santis, R., et al. (2022). Role of YAP in early ectodermal specification and a Huntington's Disease model of human neurulation. *ELife* 11, e73075. doi:10.7554/eLife.73075
- Ross, C. A., and Tabrizi, S. J. (2011). Huntington's disease: from molecular pathogenesis to clinical treatment. *Lancet Neurol.* 10 (1), 83–98. doi:10.1016/S1474-4422(10)70245-3
- Ruzo, A., Croft, G. F., Metzger, J. J., Galgoczi, S., Gerber, L. J., Pellegrini, C., et al. (2018). Chromosomal instability during neurogenesis in Huntington's disease. *Development* 145 (2), dev156844. doi:10.1242/dev.156844
- Saudou, F., and Humbert, S. (2016). The biology of huntingtin. *Neuron* 89 (5), 910–926. doi:10.1016/j.neuron.2016.02.003
- Schmidt, U., Weigert, M., Broaddus, C., and Myers, G. (2018). "Cell detection with star-convex polygons," in *Medical Image Computing and Computer Assisted Intervention—MICCAI 2018*. Editors A. F. Frangi, J. A. Schnabel, C. Davatzikos, C. Alberola-López, and G. Fichtinger (Springer International Publishing) 11071, 265–273. doi:10.1007/978-3-030-00934-2_30
- Schobel, S. A. (2021). *Preliminary results from GENERATION HD1, a Phase III trial of tominersen in individuals with manifest Huntington's disease*. Available at: <https://medically.gene.com/global/en/unrestricted/neuroscience/CHDI-2021/chdi-2021-presentation-schobel-an-update-from-the-tomin.html>.
- Shirendeb, U. P., Calkins, M. J., Manczak, M., Anekonda, V., Dufour, B., McBride, J. L., et al. (2012). Mutant huntingtin's interaction with mitochondrial protein Drp1 impairs mitochondrial biogenesis and causes defective axonal transport and synaptic degeneration in Huntington's disease. *Hum. Mol. Genet.* 21 (2), 406–420. doi:10.1093/hmg/ddr475
- Wennagel, D., Braz, B. Y., Capizzi, M., Barnat, M., and Humbert, S. (2022). Huntingtin coordinates dendritic spine morphology and function through cofilin-mediated control of the actin cytoskeleton. *Cell Rep.* 40 (9), 111261. doi:10.1016/j.celrep.2022.111261
- White, J. K., Auerbach, W., Duyao, M. P., Vonsattel, J.-P., Gusella, J. F., Joyner, A. L., et al. (1997). Huntingtin is required for neurogenesis and is not impaired by the Huntington's disease CAG expansion. *Nat. Genet.* 17 (4), 404–410. doi:10.1038/ng1297-404
- Zhang, Y., Leavitt, B. R., van Raamsdonk, J. M., Dragatsis, I., Goldowitz, D., MacDonald, M. E., et al. (2006). Huntingtin inhibits caspase-3 activation. *EMBO J.* 25 (24), 5896–5906. doi:10.1038/sj.emboj.7601445
- Zuccato, C., Ciammola, A., Rigamonti, D., Leavitt, B. R., Goffredo, D., Conti, L., et al. (2001). Loss of huntingtin-mediated BDNF gene transcription in Huntington's disease. *Science* 293 (5529), 493–498. doi:10.1126/science.1059581